Band alignment in GAA nanosheet structures from density dependent hybrid functional and many-body GW methods

Troels Markussen
Synopsys Denmark ApS
Copenhagen, Denmark
troels@synopsys.com

Petr A. Khomyakov
Synopsys Denmark ApS
Copenhagen, Denmark
petrk@synopsys.com

Brecht Verstichel
Synopsys Denmark ApS
Copenhagen, Denmark
brecht@synopsys.com

Anders Blom
Synopsys Inc
Mountain View, United States
andersb@synopsys.com

Rasmus Faber
Synopsys Denmark ApS
Copenhagen, Denmark
faber@synopsys.com

2024 International Conference on Simulation of Semiconductor Processes and Devices (SISPAD) | 979-8-3315-1635-2/24/$31.00 ©2024 IEEE | DOI: 10.1109/SISPAD62626.2024.10732914

***Abstract*—We present a computational study of the band alignment in GAA nanosheet structures. We present a dielectric dependent hybrid functional approach with metallic corrections that correctly predicts the band gaps of semiconductors and insulators as well as the density of states of metals. We use this method to study the band alignment of a silicon nanosheet in a GAA structure with respect to the TiN Fermi level. The band alignment is shown to be tunable by the Ge concentration in a thin $Si_{1-x}Ge_x$ cladding layer.**

Keywords—GAA, DFT, Hybrid functionals, band alignment

I. Introduction

Nanosheet gate-all-around (GAA) field effect transistor (FET) structures have emerged as promising candidates for replacing FinFETs in the next-generation transistor devices. The GAA FET architecture, where the gate fully surrounds the channel, provides superior gate control, compared to traditional planar MOSFET and FinFET devices [1]. While the GAA structures offer significant advantages, challenges remain in optimizing their geometry and ensuring device-to-device consistency [2]. Development of accurate atomistic simulation models for GAA FETs is crucial for understanding and optimizing their behavior in nanoscale dimensions.

In this paper, we present state-of-the-art density dependent hybrid (DDH) [3] density functional theory calculation for band diagram and related band offsets across the entire HKMG stack of GAA silicon nanosheet FET, as shown in Fig. 1. The DDH method implemented in the QuantumATK software package [4,5] correctly predicts the band gap of a large range of materials at a level comparable to many-body perturbation theory (MBPT) G_0W_0 calculations, also reproducing the G_0W_0 -obtained density of states for metallic TiN. This represents a quantitative improvement in quality and predictability as compared to standard HSE06 hybrid functional calculations.

II. Simulation Methods

In this work, we have used density functional theory (DFT) for studying the band alignment in silicon nanosheet GAA stack structures. All calculations have been done with the QuantumATK software package [4,5]. Structural relaxations have been performed using the generalized gradient approximation (GGA-PBE) [6] to the exchange correlation functional using a linear combination of atomic orbitals (LCAO) Medium basis set. When optimizing the atomic structure we allow the out-of-plane lattice constant to be relaxed with a stress tolerance of 0.1 GPa, but keep the in-plane lattice constant fixed at the bulk silicon value. The atomic positions are relaxed with a force tolerance of 0.05 eV/Å.

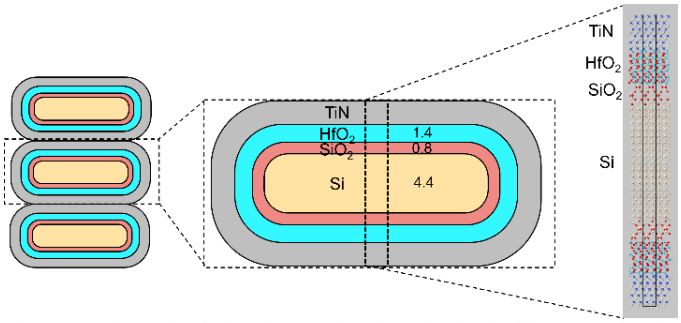

Fig. 1. We aim at simulating the central region of a single silicon nanosheet in a GAA structure with a SiO2|HfO2|TiN HKMG stack structure with thicknesses of the Si, SiO2, and HfO2 layers indicated in the central inset; the right-most inset shows the atomistic structure.

A. Density dependent hybrid functional

While GGA-PBE is well-suited for structural properties, it underestimates the band gap of dielectric materials, as compared to measured values. Using hybrid functionals, which include a fraction (α) of exact exchange interaction, greatly improves the calculated band gap values. This is particularly true for the HSE06 (α=0.25) functional used in the present study. However, the value of α is not universal, e.g., a larger value of α is required to match experimental band gap values for insulators. Here, we present our implementation of an HSE-based DDH functional, with local, position-dependent $\alpha(\boldsymbol{r})$ determined from the self-consistent electron density [3]. We introduce a Gaussian convoluted local estimator

$$\bar{g}(\boldsymbol{r}) = \frac{1}{(2\pi\sigma^2)^{3/2}} \int d^3\boldsymbol{r}' \sqrt{\frac{|\nabla\rho(\boldsymbol{r}')|}{\rho(\boldsymbol{r}')}} e^{-\frac{|\boldsymbol{r}-\boldsymbol{r}'|^2}{2\sigma^2}},$$

from which we calculate the local exchange fraction as

$$\alpha(\boldsymbol{r}) = a + b \cdot \bar{g}(\boldsymbol{r})^4,$$

where a and b are fitted to experimental band gaps for a range of semiconductors and insulators.

B. Metallic correction to local DDH

For metallic systems, HSE06 typically overestimates the band width, often leading to a too low density of states (DOS) at the Fermi level (E_F), which may also influence the band alignment, and the GGA-PBE functional is generally more accurate. This is why we introduce a second, metallic,
estimator. At every step of the self-consistent loop we calculate the Fermi level local density of states, LDOS($\boldsymbol{r}$, E_F). We then define the following metallic estimator function:

$$M(\boldsymbol{r}) = \begin{cases} 1\ , & \mathrm{LDOS}(\boldsymbol{r}, E_F) < C \\ 0\ , & \mathrm{LDOS}(\boldsymbol{r}, E_F) \geq C \end{cases}$$

where C is a cutoff value. We also convolute $M(\boldsymbol{r})$ with a Gaussian smearing function to obtain a smooth metallic estimator, $m(\boldsymbol{r})$. The final, metallic-DDH local exchange fraction is then obtained as

$$\alpha_m(\boldsymbol{r}) = \alpha(r) \cdot m(\boldsymbol{r}).$$

The LCAO HSE implementation in QuantumATK is using the pair interaction resolution of identity (PARI) approximation to the two-electron four center Coulomb integrals, which is the computational bottleneck in hybrid calculations.

C. Validation of metallic HSE-DDH

We validate the HSE-DDH obtained bandgap values for a range of semiconductor and insulator materials by benchmarking them against experimental values and bandgap values obtained with the quasi-particle MBPT-G_0W_0 method recently implemented in QuantumATK [4]; the corresponding G_0W_0 implementation details will be provided elsewhere.

As shown in Fig. 2, the results of the HSE-DDH and G_0W_0 methods are in good agreement with measured results across the entire range of bandgap values. The HSE06 functional also gives accurate results for low- to medium-gap materials, but the band gaps of wide-gap materials are underestimated by ~1 eV as shown for HfO_2 and SiO_2 oxides in Table 1.

	HSE06	HSE-DDH	G_0W_0	Reference
HfO_2	5.54	6.66	6.71	6.33[a]
SiO_2	8.63	9.81	9.68	9.65[b]

Table 1 Band gaps of HfO2 and SiO2 in units of eV. [a] Self-consistent GW value from Ref. [7]. [b] Experimental value from Ref. [8].

Fig. 3 shows bulk TiN DOS calculated with the G_0W_0, HSE06, and HSE-DDH methods, proving that the band structure values obtained using the HSE-DDH *with the additional metallic estimator* agree well with the reference G_0W_0 values.

III. Results

Having validated the HSE-DDH method as reliable for semiconductor, wide-gap insulator, and metallic materials such as TiN, we have calculated the band diagram (in terms of local DOS) and band offsets for the silicon nanosheet GAA structure with thickness of ~4.4 nm, surrounded by a SiO_2 thin layer (~0.5 nm thick), an HfO2 layer (~1.4 nm thick), and a TiN layer, as shown in Fig. 1. The energy gap regions of Si and oxides in the band diagram in Fig. 3 are indicated by the zero LDOS(z, E) in deep-black regions, whereas bright-pink regions show the highest LDOS in metallic regions. By tracing the boundaries of the zero LDOS regions, we indicate local band edges to calculate the local band gaps and band offsets.

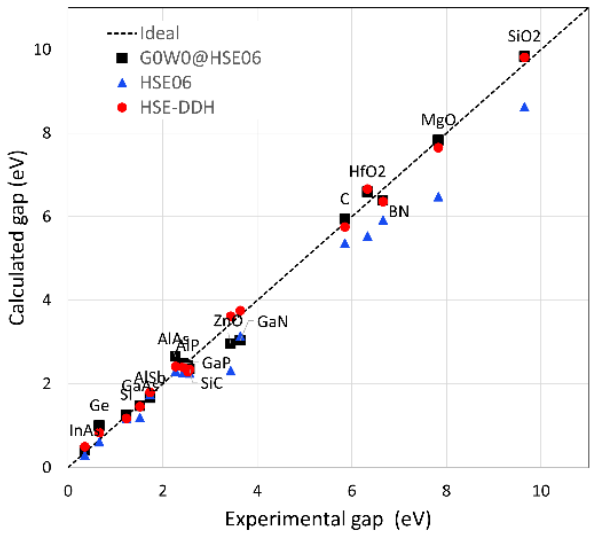

Fig. 2. Calculated vs. experimental bandgap values. The calculated data points are obtained with G_0W_0@HSE06 (black, solid line), HSE06 (blue, dot-dashed line), and HSE-DDH (red, dashed line).

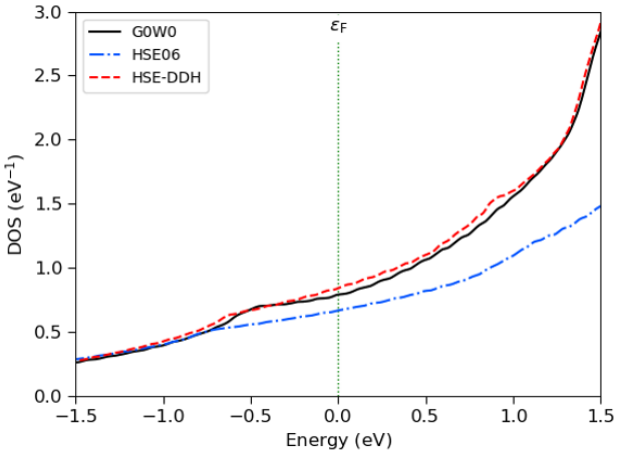

Fig. 3. TiN density of states (DOS) calculated with G_0W_0, HSE06 and HSE-DDH. The HSE06 clearly underestimates the DOS at the Fermi level compared to the G_0W_0 reference.

In the center of the Si channel, the band gap is ~1.04 eV, while the gap in the SiO_2 and HfO_2 regions are around 8.3 eV and 6.3

eV, respectively. The valence band offset (VBO) and conduction band offset (CBO) at the Si|SiO_2 interface are given in Fig. 4 and Table 2, being compared to previous calculations and measured values. The valence band maximum (VBM) in the Si channel is ~0.22 eV below the Fermi level of TiN.

The bottom inset of Fig. 4 shows the HSE-DDH calculated fraction of exact exchange (α) across the gate stack and its interfaces. For example, the α value is of ~0.25 in the Si region, as used in standard HSE06, whereas we get significantly increased α values in the HfO_2 and SiO_2 oxide regions. In the TiN metallic regions, α goes to zero as intended, essentially recovering the GGA-PBE functional value.

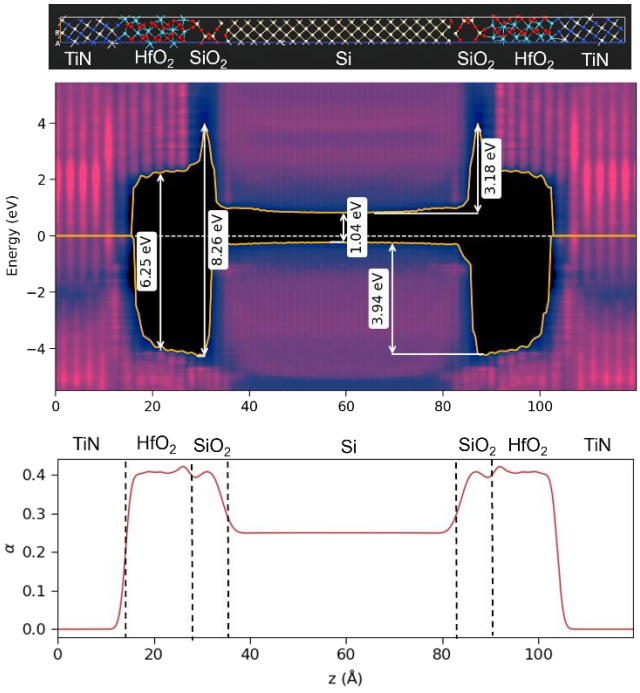

Fig. 4. Top: Atomic structure of the TiN|HfO_2|SiO_2|Si|SiO_2|HfO_2|TiN gate stack. Middle: Local density of states (LDOS) with band gaps and band off-sets indicated. The LDOS has been calculated using HSE-DDH with a Medium basis. Bottom: The exact exchange parameter as obtained from the DDH calculation.

	HSE-DDH	Ref. calc.	Experiment
VBO (eV)	4.0	4.3	4.3
CBO (eV)	3.2	3.2	3.1

Table 2 VBO and CBO between Si and SiO_2. Reference calculations and experimental values from Ref. [9] and references therein.

A. Influence of $Si_{1-x}Ge_x$ cladding layer

We continue to investigate the effect of introducing a fraction of Ge in an outer 1 nm thick cladding layer such that the channel profile looks like the one schematically shown in Fig. 5. The Ge atoms are introduced by randomly substituting some of the Si atoms. We have then calculated the LDOS for the structure where all atoms remain in their original (relaxed) positions and for a re-optimized atomic structure, where we fix the in-plane lattice constants. We do this to disentangle the effects of relaxation and pure Ge substitution. An example of the atomic structure in the channel and cladding layer is shown in Fig. 6 (top).

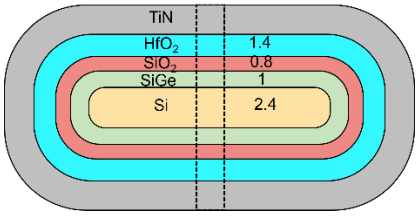

Fig. 5. Single Si|SiGe nanosheet in a GAA structure with a SiO2|HfO2|TiN HKMG stack. The numbers indicate the approximate thicknesses of each layer in units of nm.

Fig. 6 (bottom) shows the LDOS in the Si channel region for the pure Si case (left) - same LDOS as in Fig. 4, but zoomed in, and with a $Si_{0.8}Ge_{0.2}$ cladding layer (right), where the atomic structure have been re-optimized after the Ge substitutions. The addition of Ge to the cladding layer leads to local bandgap closing in the cladding layer, which is mainly driven by an upward shift of the valence band. The band gap in the center of the Si channel is slightly increased by the Ge inclusion, but the valence band maximum (VBM) in the center of the Si channel is moved down in energy.

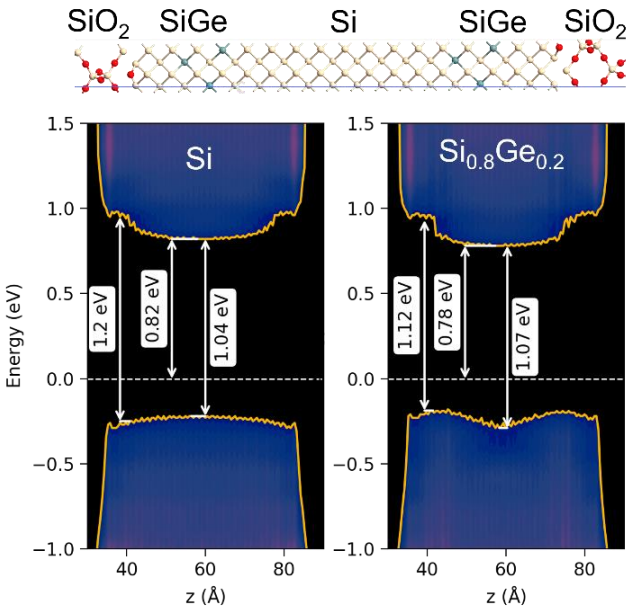

Fig. 6. Top: Atomic structure of the SiO_2|$Si_{0.8}Ge_{0.2}$|Si|$Si_{0.8}Ge_{0.2}$|SiO_2 structures in the center of the HKMG stack. Bottom: LDOS for a pure Si channel (left) and with a $Si_{0.8}Ge_{0.2}$ cladding layer (right). The LDOS is zoomed in around the Si channel Lcal band gaps in the SiGe region close to SiO2 and in the centre of the Si channel are indicated together with the Si CBM relative to the Fermi level (horizontal dashed line).

Fig. 7 shows the change of local band gap in the Si center and SiGe cladding layer for different Ge fractions calculated from re-optimized structures (solid lines) and without additional

relaxations (dashed lines). The lowering of the bandgap in the cladding layer is expected since it is well-known that the band gap in bulk $Si_{1-x}Ge_x$ decreases with increasing Ge fraction. This effect is seen to be driven completely by the structural relaxation. In the center of the Si channel a band gap increase is observed, which also is most pronounced in the re-optimized structures. These results highlight the importance of structural relaxation effects.

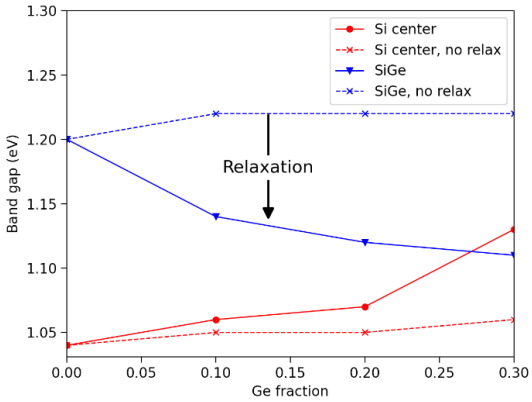

Fig. 7. Band gap vs. Ge fraction calculated from re-optimized atomic structures after Ge substitution (solid lines) and from structure with no further relaxation (dashed lines). In the $Si_{1-x}Ge_x$ cladding layer ('SiGe'), the band gap decreases with increasing Ge content due to the lower band gap of Ge. In the centre of the Si channel ('Si center') the band gap increases with Ge fraction.

Figure 8 shows the change of valence band maximum (VBM) and conduction band minimum (CBM) in the center of the Si channel, relative to the pure Si channel, as function of Ge fraction in the cladding layer. We again show results for relaxed (solid lines) and un-relaxed structures (dashed lines). We observe the largest shift for 30% Ge in the VBM with a downshift of -0.175 eV whereas the CBM is shifted by -0.075 eV. Although the band shift trends are the same in relaxed and un-relaxed structures, the effect is more pronounced in the relaxed ones, again illustrating the importance of the structural properties. The modulation of Si bands shows how careful optimization of Ge content can be used to optimize the device performance.

IV. Conclusion

We presented HSE-DDH calculations including metallic corrections for an HKMG stack of GAA silicon nanosheet FET structure. The HSE-DDH method with metallic corrections closely reproduce reference MBPT-G_0W_0 calculations for both semiconductor and insulator band gaps as well as metallic DOS. This demonstrates the improved quality and transferability of the HSE-DDH over standard HSE06 functional calculations. The calculated $Si|SiO_2$ band offsets in the considered HKMG stack model structure were found in good agreement with measured data. Introducing a fraction of Ge in a surrounding cladding layer leads to a downward energy shift of both VBM and CBM, which is mainly caused by structural relaxation effects.

The *ab initio* atomistic simulations (done at DFT and MBPT level) presented can be adopted for interpreting experimental data on material properties of gate stacks, potentially guiding the design of GAA nanosheet FETs.

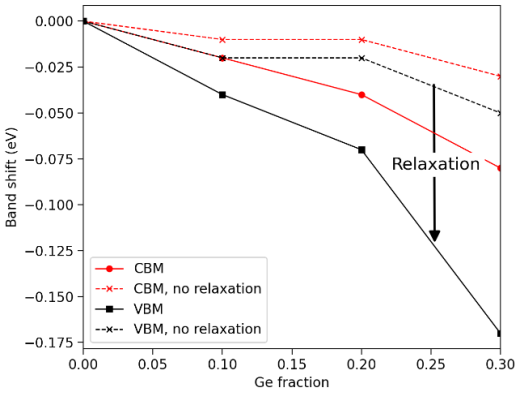

Fig. 8 Shift of VBM and CBM vs. Ge fraction, relative to the pure Si case, calculated from re-optimized structures (solid lines) and un-relaxed structures (dashed lines). Both VBM and CBM are measured in the centre of the Si channel.

References

[1] N. Loubet et al., "Stacked nanosheet gate-all-around transistor to enable scaling beyond FinFET," 2017 Symposium on VLSI Technology, Kyoto, Japan, 2017, pp. T230-T231.

[2] Mukesh, S.; Zhang, J. A Review of the Gate-All-Around Nanosheet FET Process Opportunities. Electronics 2022, 11, pp. 3589.

[3] Pedro Borlido, Miguel A. L. Marques, and Silvana Botti. "Local Hybrid Density Functional for Interfaces". Journal of Chemical Theory and Computation 2018 14 (2), 939-947.

[4] QuantumATK version V-2023.12, https://www.synopsys.com/silicon/quantumatk.html.

[5] S. Smidstrup et al., "QuantumATK: an integrated platform of electronic and atomic-scale modelling tools," Journal of Physics: Condensed Matter, 2019, vol. 32, no. 1, p. 015901

[6] J. P. Perdew, K. Burke, and M. Ernzerhof, "Generalized Gradient Approximation Made Simple", Phys. Rev. Lett. 1996, 77, pp. 3865.

[7] B. Sklénard et al. "Optical vs electronic gap of hafnia by ab initio Bethe-Salpeter equation". Appl. Phys. Lett. 2018; 113 (17)

[8] Milton, K.L.; Durrant, T.R.; Cobos Freire, T.; Shluger, A.L. "Difference in Structure and Electronic Properties of Oxygen Vacancies in α-Quartz and α-Cristobalite Phases of SiO2". Materials 2023, 16, 1382

[9] R. Shaltaf et al. " Band Offsets at the Si/SiO2 Interface from Many-Body Perturbation Theory", Phys. Rev. Lett. 2008, 100, 186401.